Physics of Hall-Effect Discharge by Particle

IEPC-2013-148
Presented at the 33rd International Electric Propulsion Conference,
The George Washington University • Washington, D.C. • USA
October 6 – 10, 2013

F. Taccogna[1] P. Minelli[2] and N. Oudini[3]
Istituto di Metodologie Inorganiche e di Plasmi - CNR, via Amendola 122/D, 70126 Bari, Italy

Abstract: **There are still many missing elements to complete the full understanding of physical mechanisms at the basis of the Hall thruster functioning. The origin of the anomalous electron cross-field transport remains unrevealed, while electron-wall interaction is often studied by local and/or reduced dimensional models. In this study, we attempt a fully kinetic self-consistent 3D particle-based simulation of the Hall-effect discharge. Results show the presence of multi-dimensional sheath structures in the acceleration region characterized by azimuthal modulation and axial transition from classical to reversed sheath.**

Nomenclature

B	=	magnetic field
e	=	elementary charge = 1.602189x10^{-19} C
E	=	electric field / energy
f	=	geometrical scaling factor
i	=	axial mesh index
I	=	current
I_D	=	discharge current
j	=	radial mesh index / current density
k	=	azimuthal mesh index / wave number
k_B	=	Boltzmann constant = 1.380662x10^{-23}
L_z	=	channel length
m	=	electron mass = 9.11x10^{-31} Kg.
M	=	ion mass (Xe) = 2.18x10^{-25} Kg.
n	=	density
r	=	radial direction
r_{in}	=	inner radius of the channel
r_{out}	=	outer radius of the channel
V_D	=	discharge voltage
v_d	=	electron azimuthal drift velocity
w	=	macro-particle weight
z	=	axial direction
γ	=	total secondary electron emission coefficient
δ	=	true-secondary electron emission coefficient
Δt	=	time step
ε_0	=	vacuum permittivity = 8.854188x10^{-12} F/m
η	=	back-scattered electron emission coefficient
θ	=	azimuthal direction
λ_D	=	Debye length

[1] Researcher, IMIP-CNR, francesco.taccogna@ba.imip.cnr.it.
[2] Researcher, IMIP-CNR, pierpaolo.minelli@ba.imip.cnr.it.
[3] Researcher, IMIP-CNR, noureddine.oudini@ba.imip.cnr.it.

π	=	pi-greek = 3.1415926536
ρ	=	charge density / re-diffused electron emission coefficient
σ	=	surface charge density / cross section
ϕ	=	electric potential
ω_p	=	electron plasma frequency
Ω	=	cyclotron frequency

I. Introduction

One of the most important open questions in the physics of Hall effect thrusters (HET) discharge concerns the electron cross-field mobility. It is nowadays well accepted to attribute the anomalous electron cross-field transport to electron drift instabilities[1] and electron-wall interaction (near-wall conductivity NWC[2]).

However, it has been recently[3] suggested that this way to distinguish different contributions to the mobility with different adjustable coefficients fail to match correctly the ion velocity profile measured by the non-intrusive laser induced fluorescence (LIF) technique. This is a strong argument supporting the conclusion that the different contributions do not necessarily add each other, but they interfere in non-linear way.

Furthermore, recent collective Thomson scattering experiment[4] have showed that in the thruster channel the azimuthal mode has important components along the magnetic field (radial) and the axial direction. This demonstrates the important correlations among the different coordinates.

Up to now low-dimensional kinetic models have been developed (1D(r) and 2D(θ,z), 2D(r,θ) 2D(r,z)[5-9]): plasma is forced to be confined in one or two dimensions. In particular, in radial and (r,θ) models, the accelerator field E_z is externally imposed while, one expects that an increase of the local conductivity would yield a decrease of the local electric field, which would reduce the drift velocity and control the possible instabilities driven by the lateral sheaths. Moreover, electrons leaving the system would be replaced by "fresh" ones, a phenomenon which would limit the amplitude of perturbations and the conductivity.

The aim of this work is to avoid these limitations and to show how all the three coordinates interfere between each other; in particular if the radial sheath dynamics is able to modulate the azimuthal behaviour and consequently if the increase of electron axial conductivity changes the acceleration field. For this reason, we concentrate our efforts in the study of plasma in the entire space without introducing any artificial anomalous conductivity.

II. General Guidelines

The computational technique used is a standard electrostatic Particle-in-Cell/Monte Carlo Collision (PIC-MCC) model[10,11]. Typical values used are reported in Tab. I.

A. Particle-in-Cell (PIC) Module

The domain, consists of the co-axial channel limited axially by the anode and the exit plane (forced to be at the cathode potential) and radially by the inner and outer walls. In order to lower the computational cost we have reduced the periodicity length to $\theta=\pi/2$. Furthermore, a geometrical scaling[12] has been applied reducing the axial and radial dimension by $f=10$ and keeping constant all the most relevant non-dimensional Knudsen and Hall parameters. The volume of every cell is smaller than the Debye sphere and the time-step is chosen such that $\omega_p \Delta t=0.3$. Realistic values of the ion mass and vacuum permittivity have been kept.

Column length	L_z = 2.5 cm
Inner radius	r_{in} = 3.45 cm
Outer radius	r_{out} = 5 cm
Propellant mass flow rate	$\dot{m}$=5 mg/s
Discharge voltage	V_d = 300 V
Discharge current	I_d = 4.5 A
Max radial magnetic field	$B_{r,max}$ = 180 G

TABLE I. Operative parameters of HET.

A prescribed axial distribution (uniform in radial and azimuthal directions) of neutral Xe atoms density[13] (Fig. 1.a):

$$n_{Xe}(z) = n_{Xe}(0) + 5x10^{18} \arctan\left[10\left(1 - \frac{z}{0.018}\right)\right] \quad (1)$$

($n_{Xe}(0)$=1x10^{19} m^{-3} and z is expressed in meters) and magnetic field map[14] (Fig. 1.b) (radial and axial components while B_θ=0) are imposed and fixed during the simulation.

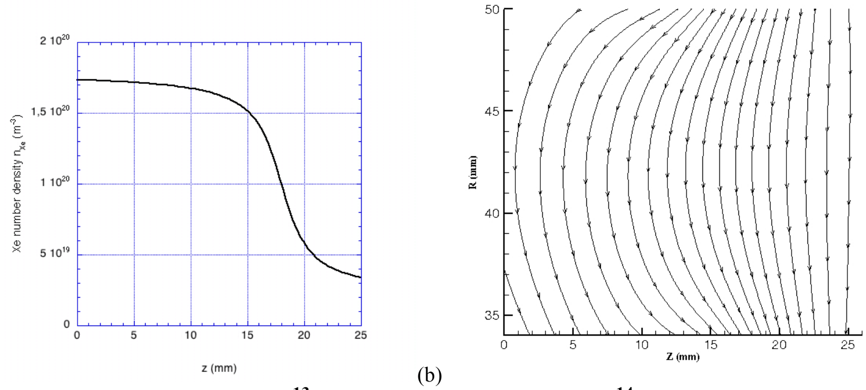

(a) (b)

Figure 1. a) Xe atoms density distribution[13] and b) magnetic field map[14] used as fixed prescribed input data in the model.

The simulation starts from an empty domain. Electrons are introduced every time step from the exit plane with half-Maxwellian (T_{e0}=20 eV) velocity distribution. The amount of electrons injected inside the channel every PIC iteration is determined by subtracting the non neutralized ion current exhausted to the current discharge ($I_{inj}=I_d-(I_{beam}-I_{e,exit})$).

The Poisson equation in three-dimensional cylindrical geometry:

$$\left(\frac{\partial^2}{\partial r^2}+\frac{1}{r}\frac{\partial}{\partial r}+\frac{1}{r^2}\frac{\partial^2}{\partial\theta^2}+\frac{\partial^2}{\partial z^2}\right)\phi(r,\theta,z)=-\frac{\rho(r,\theta,z)}{\varepsilon_0} \tag{2.a}$$

is solved with PETSc software package[15]. For this purpose, Dirichelet fixed conditions are used on axial boarders at z=0 (anode) and at $z=L_z$ (cathode):

$$\phi(r,\theta)\big|_{z=0}=V_D;\quad \phi(r,\theta)\big|_{z=Lz}=0\,, \tag{2.b}$$

while Neumann conditions are used on the insulating walls at $r=r_{in}$ and at $r=r_{out}$ (the possible surface conductivity of the dielectric is neglected):

$$\left.\frac{\partial\phi(\theta,z)}{\partial r}\right|_w \overset{def}{=} -E_{r,w}(\theta,z)=\pm\frac{\sigma_w(\theta,z)}{\varepsilon_0} \tag{2.c}$$

where + is for the outer wall and – is for the inner wall. Finally, periodic boundary conditions are set on azimuthal boundaries at θ=0 and at $\theta=\pi/2$.

B. Boundary Particle Module

Periodic conditions are used for particles crossing θ-boundaries. When an electron hits the dielectric channel wall (BN is simulated), we choose the number of electrons emitted based on its energy E_p. It is distinguished between three different types of secondary electrons: backscattered, re-diffused and true secondary electrons. A Monte Carlo probabilistic model[16] is used which allows a detailed dependence of the secondary electron emission coefficient γ on the primary electron energy E_p (see Fig. 2). A lack of data is still present in the energy range below 10 eV (a value of $\gamma(E_p=0)=0.55$ has been used). However, it should be pointed out that results are not very sensitive to the value of γ for $E_p<10$ eV because electrons hit the wall with low radial energy but still having enough azimuthal and axial component. Finally, when an ion strikes the wall it is neutralized and deleted from the list of particles tracked.

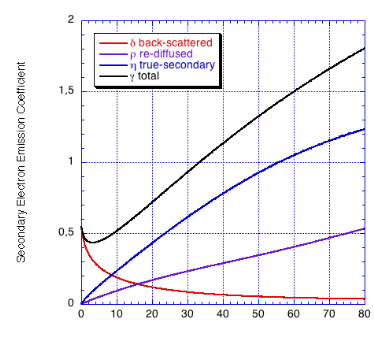

Figure 2. Secondary electron emission coefficient used in the model[16] (data correspond to BN material).

When electrons and ions leave the simulation domain from anode and cathode planes at z=0 and z=L_z, respectively, they are deleted from the list and a counter stores the number of particles in order to compute anode and cathode currents.

C. Monte Carlo Collision (MCC) Module

We apply the standard "null collision" Monte Carlo technique[17] to simulate electron-neutral (Xe) collisions, which include elastic scattering, excitation, and single ionization. Recently, it has also been suggested that the apparent discrepancy between classical and anomalous electron transport could be caused by an underestimation of ion current in simulations and experiment due to neglect of Xe^{++} doubly charged ions[18]. For this reason we have added collisions producing Xe^{++} ions such as direct double ionization of Xe atoms (cross section is reported in ref. [19]) $e + Xe \rightarrow 3e + Xe^{++}$ and single ionization of Xe^{+} ions (cross section is reported in ref. [20]) $e + Xe^{+} \rightarrow 2e + Xe^{++}$.

III. Results

The dynamical evolution of the system presents a turbulent behaviour as shown in Fig. 3, where the history of electron current arriving at the anode and ion current emitted from the exhaust plane are reported: after 2 μs a steady state is reached characterized by regular instabilities followed by quiescient phases. An instable regime suddenly appears and persists for 0.1 μs until it saturates and after a stable phase of 0.3 μs a new instability grows.

The double ionized Xe^{++} species represents less than 3% of the total ion population and the main production channel is the double ionization of atoms (80%). The current inside the thruster box is distributed in the following manner: it is almost complitely electron on the anode (about 2.42 A while the ion backflow contribution is 0.05 A) while on the exit plane the ion contribution is I_{beam}=1.36 A and the electron current injected is I_{inj}=1.04 A, that is a current ratio of η_A=0.6 is detected. Electron current collected on the lateral walls are $I_{e,in}$=2.98 A and $I_{e,out}$=7.47 A on the inner and outer wall, respectively. The corresponding secondary electron current emitted from the walls are $I_{see,in}$=2.69 A and $I_{see,out}$=7.08 A, respectively. As a consequence, secondary emission coefficient is γ_{in}=0.9 for the inner wall and γ_{out}=0.95 for the outer wall. These values are averaged along the entire axial lenght of the channel. Actually, in the last part of the acceleration region, an inversed sheath has been observed (see Fig. 6) clear sign of a lager secondary electron emission coefficient in this region.

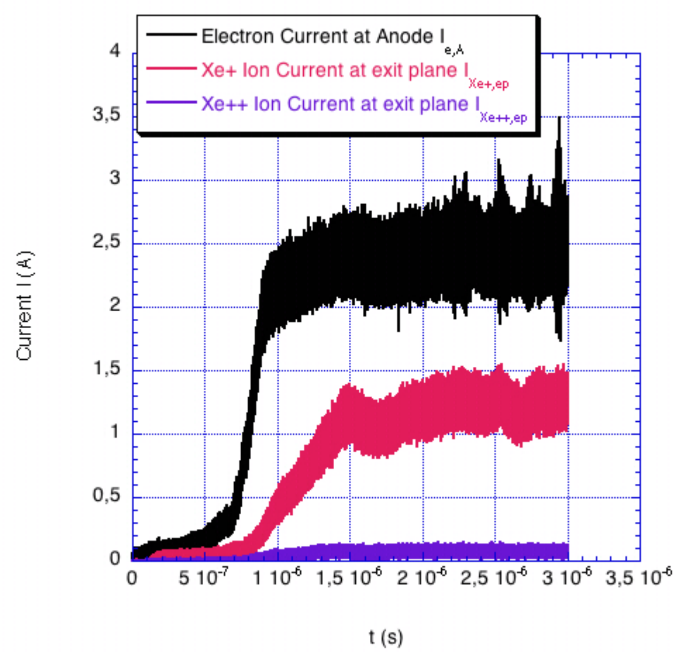

Figure 3. Temporal evolution of electron $I_{e,A}$ and ion $I_{Xe+/Xe++,ep}$ currents detected at the anode and exit plane, respectively.

Figs. 4 and 5 show a) electric potential ϕ(V), b) electron density n_e(m^{-3}) and c) electron temperature T_e(eV) distributions in {r-z} plane (at $\theta=\pi/4$) and {r-θ} plane (at z=1.9 cm), respectively. These quantities allow us to qualify and validate the model. In fact, all the most important features of the Hall discharge have been reproduced with a good agreement with previous models and measurements.

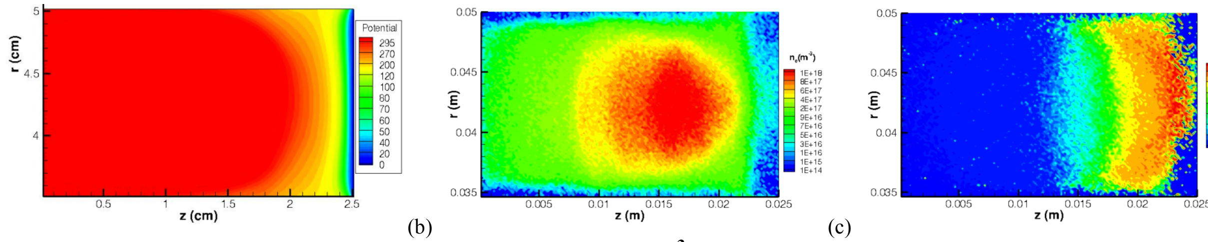

(a) (b) (c)

Figure 4. a) Electric potential ϕ(V) , b) electron density $n_e(m^{-3})$ and c) temperature T_e (eV) in the *r-z* plane (at $\theta=\pi/4$).

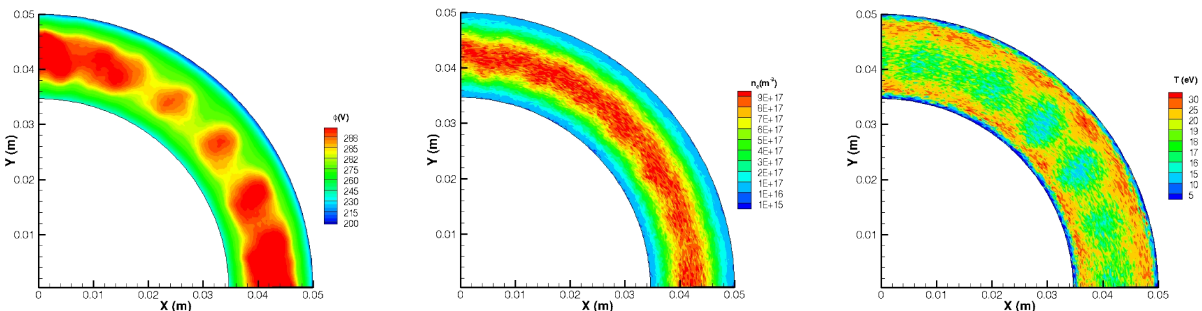

(a) (b) (c)

Figure 5. a) Electric potential ϕ(V) , b) electron density $n_e(m^{-3})$ and c) temperature T_e (eV) in the *r-θ* plane (at *z*=1.9 cm).

The axial distribution shows the acceleration field in the last fifth part of the channel length where the electron temperature reaches its maximum value of T_e=40 eV at z=2.2 cm.

The radial behaviour (in Fig. 6 electric potential radial profiles at different axial locations and $\theta=\pi/4$ have been reported) shows a very slight asymmetry between inner and outer wall. Inverted sheaths are detected in the acceleration region (z-index i>148) where a strong secondary electron emission due to the high ExB drift occurs. However, it has to be pointed out that these results could suffer from the strong boundary condition imposed on the exit plane.

The azimuthal behaviour shows the presence of a fluctuation (see Figs. 7 where the azimuthal profile of electric potential at z=1.9 cm inside the inner and outer sheaths have been reported) characterized by a wave vector $|\boldsymbol{k}|$=1263 m^{-1} and directed mostly along θ with a small radial component (see Fig. 5a). The fluctuation azimuthally modulates the sheaths which result then to have a complete three-dimensional structure.

IV. Conclusion

In this work a 3D fully kinetic PIC-MCC model of a Hall-effect discharge has been developed. The model includes double ionized Xe^{++} specie and a detailed secondary electron emission module using a geometrical scaling methodology. The model is able to capture all the most relevant features of the discharge: the acceleration field, inverted lateral sheaths and azimuthal fluctuations in the acceleration region of the channel.

Future work will concern the inclusion of the near field plume region[21] (10 cm downstream of the exit plane).

Acknowledgments

This research has received funding from Regione Puglia under grant agreement HXGY200 Progetto Hall "Aiuti a Sostegno dei Partenariati Regionali per l'Innovazione".

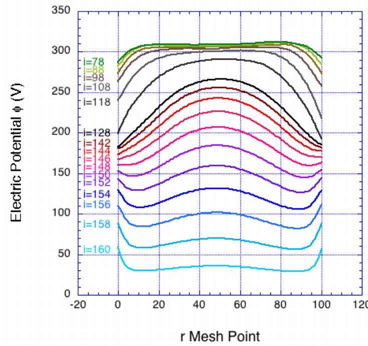

Figure 6. Radial profiles of electric potential ϕ(V) at different axial locations and $\theta=\pi/4$. The index i corresponds to the mesh point in the axial direction.

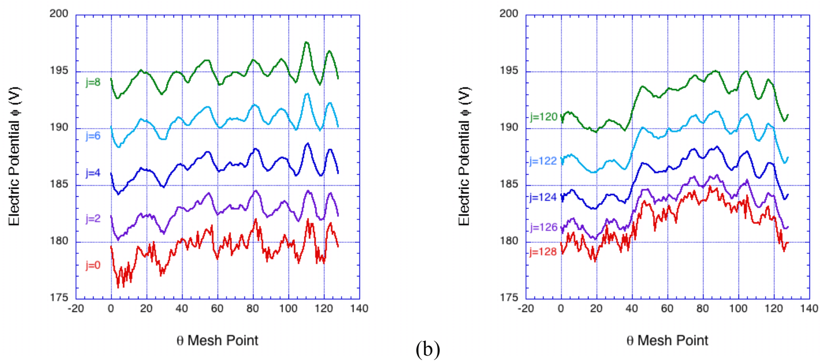

(a) (b)

Figure 7. Azimuthal profiles of electric potential ϕ(V) inside the a) inner and b) outer sheaths for *z*=1.9 cm. The index j corresponds to the mesh point in the radial direction.

References

[1]Ducrocq, A., Adam, J. C., Héron, A., and Laval, G., "High-frequency electron drift instability in the cross-field configuration of Hall thrusters", *Phys. Plasmas,* Vol. 13, 102111, 2006.

[2]Morozov, A. I., and Savel'ev, V. V., *Reviews of Plasma Physics* Vol. 21, ed. B. B. Kadomtsev and V. D. Shafranov, New York, 2000, pp. 203.

[3]Garrigues, L., Mazzoufre, S. and Bourgeois, G., "Computed versus measured ion velocity distribution functions in a Hall effect thruster", *J. Appl. Phys.*, Vol. 111, 113301, 2012.

[4]Tsikata, S., Honoré, C., Lemoine, N., and Grésillon, D. M., "Three-dimensional structure of electron density fluctuations in the Hall thrusters plasma: ExB mode", *Phys. Plasmas*, Vol. 17, 2010, 112110.

[5]Adam, J. C., Héron, A., and Laval, G., "Study of stationary plasma thrusters using two-dimensional fully kinetic simulations", *Phys. Plasmas*, Vol. 11, No. 1, 2004, pp. 295-305.

[6]Taccogna, F., Longo, S., Capitelli, M., and Schneider, R., "Plasma flow in a Hall thruster," *Phys. Plasmas*, Vol. 12, 2005, 43502.

[7]F. Taccogna, R. Schneider, S. Longo, and M. Capitelli, *Plasma Sources Sci. Technol.* 17, 024003 (2008).

[8]D. Sydorenko, A. Smolyakov, I. Kaganovitch, and Y. Raitses, *Phys. Plasmas* 15, 053506 (2008).

[9]Héron, A., and Adam, J. C., "Anomalous conductivity in Hall thrusters: Effects of the non-linear coupling of the electron-cyclotron drift instability with secondary electron emission of the walls", *Phys. Plasmas*, Vol. 20, 082313, 2013.

[10]Eastwood, J. W., and Hockney, R. W., *Computer Simulation using Particle*, McGraw-Hill, New York, 1981.

[11]Birdsall, C. K., and Langdon, A. B., *Plasma Physics via Computer Simulation*, McGraw-Hill, New York, 1985.

[12]Taccogna, F., Longo, S., Capitelli, M., and Schneider, R., "Self-similarity in Hall plasma discharge. Application to particle models", *Phys. Plasmas*, Vol. 12, 2005, 053502.

[13]Garrigues, L., "Modelisation d'un Propulseur à Plasma Stationnaire pour Satellites", PhD Thesis, Universitè Paul Sabatier, Toulouse, 1998.

[14]Matyash, K., *private communication*, 2011.

[15]PETSc, Portable, Extensible Toolkit for Scientific Computation, Software Package, Vers. 3.1, Argonne Nationa Laboratory, http://www.mcs.anl.gov/petsc/petsc-as/

[16]Furman, M. A., Pivi, M. T. F., "Probabilistic model for the simulation of secondary electron emission", *Phys. Rev. Special Topics–Accel. and Beams*, Vol. 5, 2002, 124404.

[17]Vahedi, V., Surendra, M., "A Monte Carlo collision model for particle-in-cell method: applications to argon and oxygen discharges", *Comp. Phys. Comm.,* Vol. 87, 1995, pp. 179-198.

[18]Katz, I., Hofer, R., and Goebel, D., "Ion Current in Hall Thrusters", IEPC-2007-365.

[19]Jha L. K., Santosh Kumar, Roy, O. P., and Kumar, P., "Single and double ionization of Kr and Xe by electron impact", *Phys. Scripta*, Vol. 77, 2008, 015304.

[20]Bell, E. W., Djuric, N., and Dunn, G. H., "Electron-impact ionization of In^+ and Xe^+", *Phys. Rev. A*, Vol. 48, No. 6, 1993, pp. 4286-4291.

[21]Oudini, N., Taccogna, F., and Minelli, P., "3D Fully Kinetic Simulation of Near-Field Plume Region", *IEPC-2013-419*.